



# Supramolecular Assemblies with Near-Infrared Emission Mediated in Two Stages by Cucurbituril and Amphiphilic Calixarene for Lysosome-Targeted Cell Imaging

Xu-Man Chen, Yong Chen, Qilin Yu, Bo-Han Gu, and Yu Liu\*

**Abstract:** A two-stage mediated near-infrared (NIR) emissive supramolecular assembly for lysosome-targeted cell imaging is presented. 4,4'-Anthracene-9,10-diylbis(ethene-2,1-diyl)bis(1-ethylpyridin-1-ium) bromide (ENDT) was synthesized as an organic dye with weak fluorescence emission at 625 nm. When ENDT complexes with cucurbit[8]uril (CB[8]), this binary supramolecular complex assembles into nanorods with a near-infrared fluorescence emission (655 nm) and fluorescence enhancement as the first stage. Such supramolecular complexes interact with lower-rim dodecyl-modified sulfonatocalix[4]arene (SC4AD) to form nanoparticles for further fluorescence enhancement as the second stage. Furthermore, based on a co-staining experiment with LysoTracker Blue, such nanoparticles can be applied in NIR lysosome-targeted cell imaging.

Supramolecular self-assemblies with fluorescence for cell imaging have attracted raising attention of chemists in recent years,<sup>[1]</sup> especially for organelle-targeted cell imaging. Among various organelles in cells, lysosome is an important organelle that is involved in various cell processes, including degradation of polymers, secretion, plasma membrane repair, cell signaling, and energy metabolism.<sup>[2]</sup> Several lysosome-targeted probes have been reported based on rhodamine<sup>[3]</sup> and ruthenium complexes.<sup>[4]</sup> On the other hand, as for good utilization of various functions of fluorescent supramolecular assemblies, near-infrared (NIR) fluorescent assemblies (650–900 nm) is widely used owing to its various advantages in cell imaging,<sup>[5]</sup> mainly because NIR fluorescent emission can get very slight photo-damage on biological samples, minimum interference from biomolecule autofluorescence, and deep tissue penetration.<sup>[6]</sup> However, such NIR emission supramolecular assembly are lacked because the emission of organic dyes cannot usually reach NIR as well as aggregation induced quenching (ACQ) in assemblies.

In supramolecular self-assemblies, some fluorescence-silent organic dyes could be induced to undergo various fluorescence emissions mainly by two methods: host–guest

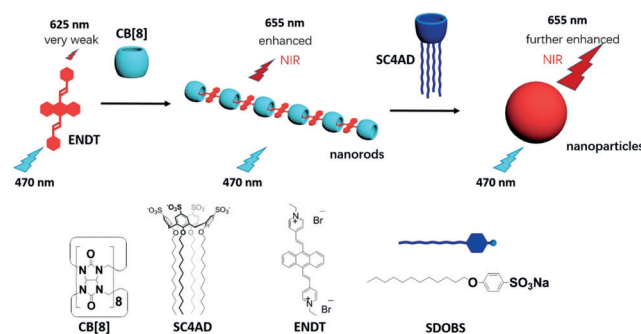
complexation<sup>[7]</sup> and aggregation-induced emission (AIE).<sup>[8]</sup> Furthermore, some dyes with fluorescence could undergo a shift of its emission wavelengths by such methods. In supramolecular assemblies, organic dyes usually form J-aggregates or H-aggregates resulting in the changes in emission intensity or wavelength.<sup>[9]</sup> In J-aggregates, emissions of organic fluorescent dyes usually undergo red-shift and enhancement, whereas they usually undergo blue-shift and quenching in H-aggregates.

Cucurbituril<sup>[10]</sup> and calixarene,<sup>[11]</sup> two types of host macrocyclic compounds, are usually used for the design of supramolecular assemblies. Among various types of cucurbituril, cucurbit[8]uril (CB[8]) can usually complex with two guest molecules, which is easily to form supramolecular aggregates.<sup>[12]</sup> Furthermore, amphiphilic *p*-sulfonatocalix[4]arene, a kind of water-soluble calixarene, are usually used for supramolecular assemblies due to calixarene induced aggregation (CIA).<sup>[13]</sup> Thus, an anthracyl pyridinium derivative (ENDT) has been designed with very weak fluorescence emission at 625 nm, which undergoes the first-stage emission enhancement and red-shift to NIR (655 nm) owing to J-aggregation by being included in CB[8], and the ENDT/CB[8] assemblies into nanorods. Such supramolecular aggregates further assemble with lower-rim dodecyl-modified sulfonatocalix[4]arene (SC4AD) into nanoparticles, to realize the second-stage enhancement of NIR emission (Scheme 1). When ENDT&CB[8] binary aggregates mix with same concentration of charges of sodium *p*-dodecyloxy benzene sulfonate (SDOBS) as SC4AD, emission cannot be further enhanced. Thus, we have achieved near-infrared emissive supramolecular assemblies mediated in two-stages by CB[8] and SC4AD. Furthermore, while ENDT assembles with only SC4AD, fluorescence emission wavelength will undergo blue-shift to 600 nm because ENDT molecules are included in the

[\*] X. M. Chen, Dr. Y. Chen, Q. L. Yu, B. H. Gu, Prof. Y. Liu  
College of Chemistry, State Key Laboratory of Elemento-Organic Chemistry, Nankai University  
Tianjin 300071 (P. R. China)  
E-mail: yuliu@nankai.edu.cn

Dr. Y. Chen, Prof. Y. Liu  
Collaborative Innovation Center of Chemical Science and Engineering (Tianjin)  
Tianjin 300072 (P. R. China)

Supporting information and the ORCID identification number(s) for the author(s) of this article can be found under:  
<https://doi.org/10.1002/anie.201807373>.



**Scheme 1.** Illustration of NIR fluorescent supramolecular assemblies and related supramolecular aggregates.

cavities of SC4AD, and emission is enhanced because of CIA and AIE. Furthermore, according to co-staining experiment with LysoTracker Blue, such nanoparticles with NIR emissions can be used as targeted imaging agents for lysosome in living cells.

First, we need to characterize the recognition motif of ENDT/CB[8] complexes. It has been well-established that CB[8] can complex with guests with positive charge. There are two positive charged pyridinium groups in one ENDT molecule. Because of the large cavity in CB[8], one CB[8] molecule usually includes two derivate pyridinium groups. Therefore, the inclusion complexation between ENDT with CB[8] was investigated. Job's plot confirmed that ENDT/CB[8] complexes adopted a 1:1 stoichiometry ostensibly (Supporting Information, Figure S1), but there are three possible binding motifs of ENDT/CB[8] complexes: simple 2:2 binding motif (Figure 1a), stacked  $n:n$  binding motif

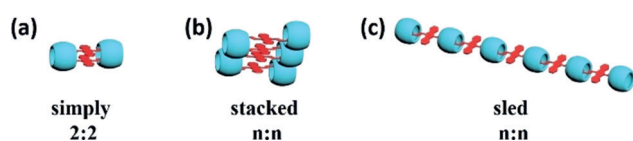


**Figure 1.** Illustration of three possible binding motifs between ENDT and CB[8].

(Figure 1b), and sled  $n:n$  motif (Figure 1c). To determine which binding motif is occurring, a UV/Vis absorbance titration of ENDT in the presence of varying concentrations of CB[8] was investigated. In Figure 2b and the Supporting Information, Figure S2, upon raising the concentration of CB[8], UV/Vis absorbance of ENDT underwent a red-shift from 461 nm to 515 nm, which indicates ENDT molecules form J-aggregates after binding with CB[8]. Because of the different spectral changes at 480–500 nm (Supporting Information, Figure S2), we can infer that there are multiple

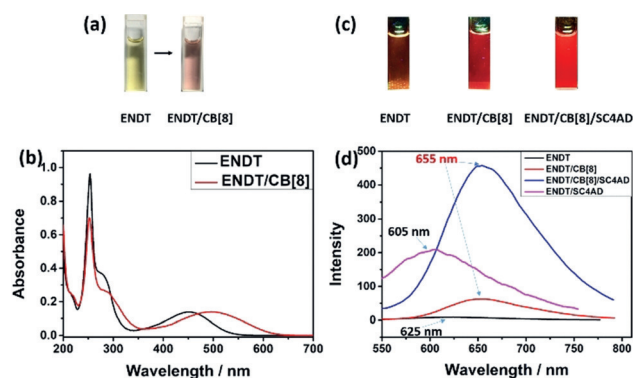


**Figure 2.** a) Photographs of aqueous ENDT (0.02 mM) and ENDT/CB[8] ([ENDT]=[CB[8]]=0.02 mM). b) UV/Vis spectra of ENDT (0.02 mM) and ENDT/CB[8] ([ENDT]=[CB[8]]=0.02 mM) in aqueous solution at 25 °C. c) Photographs of fluorescence of ENDT, ENDT/CB[8] and ENDT/CB[8]/SC4AD under 395 nm light. ([ENDT]=[CB[8]]=0.02 mM, [SC4AD]=0.04 mM, respectively). d) Fluorescence emission spectra of ENDT, ENDT/CB[8], ENDT/CB[8]/SC4AD, and ENDT/SC4AD. [ENDT]=[CB[8]]=0.02 mM, [SC4AD]=0.04 mM,  $\lambda_{\text{ex}} = 470$  nm.

complex species during the complexation by gradually adding CB[8], especially 2:1 ENDT/CB[8] complexes. Because simply 2:2 binding motif as well as stacked  $n:n$  binding motif can easily induce ENDT molecules to form H-aggregates while sled binding motif usually induce ENDT molecules to form J-aggregates, the binding motif of ENDT/CB[8] complexes should be a sled  $n:n$  binding motif. ENDT aqueous solution appears light yellow (Figure 2a), and changes into light pink when one equiv of CB[8] is added, which is another expression for confirming formed J-aggregates of ENDT/CB[8]. Furthermore, in  $^1\text{H}$  NMR spectra of ENDT with varying concentrations of CB[8] (Supporting Information, Figure S3), peaks related to protons  $\text{H}_{\text{a,b,c,d,g,h}}$  shifted upfield and broaden owing to inclusion into CB[8] and stacking, while peaks related to protons  $\text{H}_{\text{e,f}}$  of anthracene groups possess little shift, which indicates that anthracene groups do not stack when complexing with CB[8]. 2D NOESY (Supporting Information, Figure S4) showed clear NOE effects between the protons of ethyl pyridinium groups (protons a, b, g, h) in ENDT and the protons of CB[8], indicating that the positively charged ethyl pyridinium groups of ENDT were included in the cavity of CB[8]. Furthermore, on the basis of the UV/Vis absorbance titration, the association constants ( $K_{\text{a}}$ ) could be calculated as  $(1.04 \pm 0.12) \times 10^6 \text{ L mol}^{-1}$  for ENDT/CB[8] using a nonlinear least-squares curve-fitting method (Supporting Information, Figure S5).

After we determined the ENDT/CB[8] recognition motif, another macrocycle molecule, SC4AD is used to interact with ENDT/CB[8] aggregates. Fixing  $[\text{ENDT}] = [\text{CB[8]}] = 0.02 \text{ mM}$  (Supporting Information, Figure S6b,c), when [SC4AD] raised to 0.01 mM, there is a deep decrease of transmittance (Supporting Information, Figure S6b, blue and light gray lines), meaning that they can assemble completely owing to the same number of positive and negative charges. When the concentration of SC4AD continuously raised, excess SC4AD can encase ENDT/CB[8] aggregates into its hydrophobic layer and the transmittance increased back. When [SC4AD] was more than 0.03 mM, it is above the critical aggregation concentration (CAC) of SC4AD itself,<sup>[14]</sup> so transmittance decreased gradually (Supporting Information, Figure S6b, pink and purple lines). Tyndall experiments can also prove such transmittance results. In the Supporting Information, Figure S6a, there is nearly no Tyndall effect of aqueous ENDT, and slight Tyndall effect of ENDT/CB[8], while there is a strong Tyndall effect of ENDT/CB[8]/SC4AD.

Fluorescence experiment has been done to determine the red-shift of ENDT after complexing with CB[8] and the enhancement after assembling with SC4AD. In Figures 2c and d, the max emission wavelength of ENDT is 625 nm with weak emission band. This weak emission is mainly caused by  $\pi$ - $\pi$  stack of anthracene groups and intermolecular charge transfer between anthracene group and pyridinium group. After adding CB[8], the maximum emission wavelength shifted to 655 nm with obvious enhancement, which leads a stronger NIR emission. The gradually titration experiments are shown in the Supporting Information, Figures S7 and S8. In aqueous solution of ENDT/CB[8], the positively charged pyridinium groups were threaded into the cavity of CB[8], so that the rotation of single C–C bond between pyridinium and

anthracene group is limited, and the fluorescence is enhanced. Furthermore, owing to steric hindrance, it is difficult for the pyridinium group and anthracene group to be in the same plane, in other words, it is difficult for ENDT molecules to have a stacked binding motif. Thus, each CB[8] molecule includes two pyridinium groups from different ENDT molecules and the inclusion mode is a sled  $n:n$  binding motif. Therefore, this inclusion mode avoids  $\pi-\pi$  stacking of anthracene groups and intermolecular charge transfer between the anthracene group and pyridinium group. Such an inclusion mode can lead ENDT/CB[8] to form J-aggregates, so that emission red-shifts to 655 nm and initially enhanced. Then, SC4AD was added into ENDT/CB[8] aggregates, to make the second-stage enhancement of fluorescence. When SC4AD was added, it can assemble with ENDT/CB[8] aggregates to limit the rotation of single bond in ENDT as well as to provide a hydrophobic environment to enhance the emission of ENDT, and both these two conditions can lead enhancement of fluorescence. As contrast experiments, we also determined the fluorescence when adding the same concentration of negative charges of SDOBS as SC4AD in ENDT/CB[8] aggregates, which expressed no obvious enhancement of fluorescence (Supporting Information, Figure S9). However, there may be a competitive inclusion between SC4AD and CB[8]. To confirm that in ENDT/CB[8]/SC4AD assemblies, ENDT is included in CB[8] rather than SC4AD, we added the same concentration of SC4AD to only aqueous ENDT, and the fluorescence was enhanced with a blue-shift of max emission to 605 nm, which is different from 655 nm emission when included in CB[8] (Figure 2d). Because the emission is still enhanced when ENDT interacted only with SC4AD, it can confirm that SC4AD can provide a hydrophobic and molecular-rotation-limited environment for enhancement of ENDT while fluorescence underwent a blue-shift owing to ENDT molecules included into the cavity of SC4AD. For a further demonstration, we added an excess (10 equiv) of SC4AD into ENDT/CB[8] aggregates to find that the fluorescence also blue-shift to 605 nm, which agrees with fluorescence of ENDT/SC4AD (Supporting Information, Figure S10). When SC4AD is excessive, ENDT can be included into the cavity of SC4AD instead of CB[8], which lead to a blue-shift of the fluorescence. Furthermore, UV/Vis absorbance experiments confirm that when SC4AD was added twice the concentration of [CB[8]], absorbance of ENDT at about 500 nm is nearly unchanged, indicating that ENDT molecules were still included in the cavities of CB[8] (Supporting Information, Figure S11). Thus, adding SC4AD cannot destroy the ENDT/CB[8] fluorophore but further enhances the NIR emission of ENDT/CB[8] to some extent by not only increasing the microenvironmental hydrophobicity around the fluorophore but also shielding the fluorophore from the deactivating water attack. We find when [SC4AD] is 2 times than [CB[8]], the fluorescence is enhanced most with NIR emission, which is the best condition of ENDT/CB[8]/SC4AD NIR fluorescence enhancement system. However, excess SC4AD will lead to blue-shift of fluorescence.

Additionally, we have determined the morphology of NIR enhancement supramolecular assemblies. Scanning electron

microscopy (SEM) and transmission electron microscopy (TEM) were employed to give the visual information of the binary ENDT/CB[8] assemblies and ENDT/CB[8]/SC4AD assemblies. In both SEM and TEM images (Figure 3a,b), we

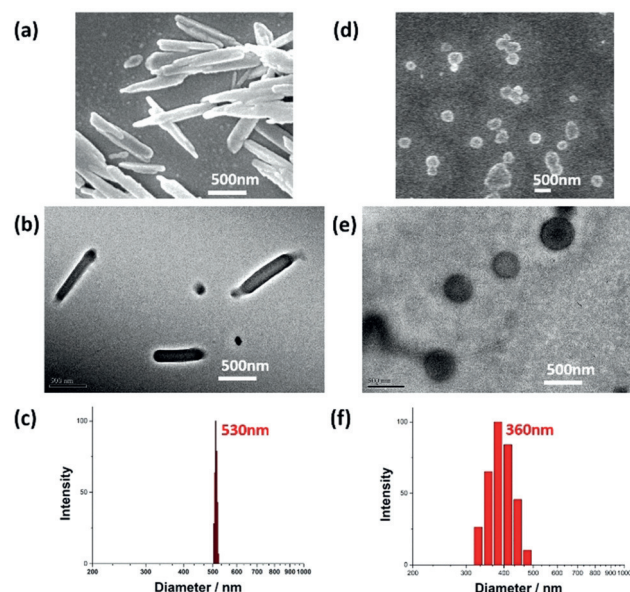


**Figure 3.** a),b),c) SEM and TEM images and DLS data of ENDT/CB[8]. ([ENDT] = [CB[8]] = 0.02 mM.) d),e),f) SEM and TEM images and DLS data of ENDT/CB[8]/SC4AD. [ENDT] = [CB[8]] = 0.02 mM, [SC4AD] = 0.04 mM.

can see several nanorods of ENDT/CB[8] assemblies. This morphology is formed mainly because sled inclusion mode of ENDT in the cavity of CB[8] can form linear supramolecular complexes, and many linear supramolecular complexes can stack with each other for final nanorods (Supporting Information, Figure S12). XRD patterns (Supporting Information, Figure S13) also indicated an ordered array of ENDT/CB[8]. When it comes to ENDT/CB[8]/SC4AD ternary assemblies (Figures 3d,e), there are several supramolecular nanoparticles in the view of both SEM and TEM images, mainly because ENDT/CB[8] aggregates with amphiphilic SC4AD and electrostatic interaction between them. Dynamic light scattering experiments (DLS) were tested for further demonstration at a scattering angle of 90°. The average hydrodynamic diameters of nanorods formed by ENDT/CB[8] is 530 nm, while the average hydrodynamic diameters of nanoparticles formed by ENDT/CB[8]/SC4AD is 360 nm, which consists of the length and width of the nanorods and the diameter of the nanoparticles. (Figure 3c,f) Therefore, nanorods formed by ENDT/CB[8] can achieve NIR emission and primarily enhance the emission, and the supramolecular amphiphilic nanoparticles possess further enhanced NIR fluorescence emission.

Furthermore, we wondered whether such nanoparticles could be utilized in biological or diagnostic fields. Thus, we have detected cell imaging properties of the nanoparticles. We treated human lung adenocarcinoma cells (A549 cells) with ENDT/CB[8]/SC4AD nanoparticles for 4 h. We then used

confocal laser scanning microscopy to determine the intracellular distribution of the ENDT/CB[8]/SC4AD assemblies. As contrast experiments, we have also treated A549 cells with ENDT, ENDT/CB[8], ENDT/CB[8]/SDOBS solutions for 4 h, respectively, and then used confocal laser scanning microscopy to detect the fluorescent assemblies as well. Only A549 cells treated with ENDT/CB[8]/SC4AD exhibited bright red fluorescence in the cytoplasm of the cells (Supporting Information, Figure S14). To further study the subcellular distribution of ENDT/CB[8]/SC4AD nanoparticles, A549 cells were co-stained with ENDT/CB[8]/SC4AD and commercially available lysosome staining dye LysoTracker Blue. In Figure 4, owing to merged purple dyeing

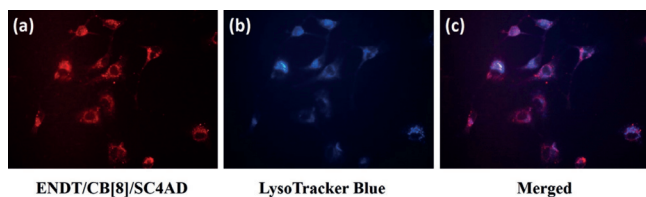


**Figure 4.** Confocal fluorescence images of A549 cells co-stained with ENDT/CB[8]/SC4AD ([ENDT]=[CB[8]]=0.005 mM, [SC4AD]=0.01 mM) and LysoTracker Blue (0.005 mM) for 30 min. a) ENDT/CB[8]/SC4AD (Ex. 470 nm, Em. 655 nm). b) LysoTracker Blue (Ex. 365 nm, Em. 450 nm). c) Merged image of (a) and (b).

site of red ENDT/CB[8]/SC4AD and blue LysoTracker Blue, it shows that ENDT/CB[8]/SC4AD and LysoTracker Blue were in good co-localization. Furthermore, cytotoxicity of ENDT/CB[8]/SC4AD nanoparticles have been evaluated. A549 cells were incubated with ENDT/CB[8]/SC4AD for 24 h, then the cell viability was measured by MTT assays. When concentration was under 0.08 mM ([ENDT]=[CB[8]]=0.08 mM, [SC4AD]=0.16 mM, respectively), the nanoparticles showed negligible toxicity to A549 cells (Supporting Information, Figure S15). Because of the high coincidence of stained position between ENDT/CB[8]/SC4AD and LysoTracker Blue, these results provide a convenient pathway for co-staining lysosomes in living cells.

In summary, supramolecular self-assemblies with two-stage NIR fluorescence enhancement were developed by employing the host-guest complex ENDT/CB[8] and further assembled with SC4AD. In contrast to nanorods formed by ENDT/CB[8], ENDT/CB[8]/SC4AD can form supramolecular amphiphilic nanoparticles. ENDT shows relatively weak emission without NIR, while nanorods formed by ENDT/CB[8] provide NIR emission with emission enhancement for the first stage. Furthermore, by assembling with SC4AD to form supramolecular nanoparticles, such NIR emission is enhanced for the second stage. Furthermore, such results proved that the dual macrocycles could cooperate to construct supramolecular assemblies for lysosome-targeted imaging in living cells.

## Acknowledgements

We thank NNSFC (21672113, 21432004, 21772099, 21861132001, and 91527301) for financial support.

## Conflict of interest

The authors declare no conflict of interest.

**Keywords:** amphiphilic calixarenes · cucurbituril · lysosome-targeted cell imaging · near-IR supramolecular assemblies

**How to cite:** *Angew. Chem. Int. Ed.* **2018**, *57*, 12519–12523  
*Angew. Chem.* **2018**, *130*, 12699–12703

- [1] a) H. Peng, L. Niu, Y. Chen, L. Wu, C. Tung, Q. Yang, *Chem. Rev.* **2015**, *115*, 7502–7542; b) C. G. Palivan, R. Goers, A. Najer, X. Zhang, A. Cara, W. Meier, *Chem. Soc. Rev.* **2016**, *45*, 377–411; c) Y. Li, Y. Dong, X. Miao, Y. Ren, B. Zhang, P. Wang, Y. Yu, B. Li, L. Isaacs, L. Cao, *Angew. Chem. Int. Ed.* **2018**, *57*, 729–733; *Angew. Chem.* **2018**, *130*, 737–741.
- [2] C. Settembre, A. Fraldi, D. L. Medina, A. Ballabio, *Nat. Rev. Mol. Cell Biol.* **2013**, *14*, 283–296.
- [3] a) D. Zhang, Y. Zheng, H. Zhang, L. He, C. Tan, J. Sun, W. Zhang, X. Peng, Q. Zhan, L. Ji, Z. Mao, *Nanoscale* **2017**, *9*, 18966–18976; b) H. Yu, Z. Hao, H. Peng, R. Rao, M. Sun, A. W. Ross, C. Ran, H. Chao, L. Yu, *Sens. Actuators B* **2017**, *252*, 313–321.
- [4] a) H. Zhang, J. Liu, C. Liu, P. Yu, M. Sun, X. Yan, J. Guo, W. Guo, *Biomaterials* **2017**, *133*, 60–69; b) S. Shen, X. Zhang, Y. Ge, Y. Zhu, X. Lang, X. Cao, *Sens. Actuators B* **2018**, *256*, 261–267.
- [5] a) P. Anees, S. Sreejith, A. Ajayaghosh, *J. Am. Chem. Soc.* **2014**, *136*, 13233–13239; b) X. Hu, J. Hu, J. Tian, Z. Ge, G. Zhang, K. Luo, S. Liu, *J. Am. Chem. Soc.* **2013**, *135*, 17617–17629; c) B. Shi, K. Jie, Y. Zhou, J. Zhou, D. Xia, F. Huang, *J. Am. Chem. Soc.* **2016**, *138*, 80–83.
- [6] a) R. Weissleder, M. J. Pittet, *Nature* **2008**, *452*, 580–589; b) Y. Liu, M. Chen, T. Cao, Y. Sun, C. Li, Q. Liu, T. Yang, L. Yao, W. Feng, F. Li, *J. Am. Chem. Soc.* **2013**, *135*, 9869–9876.
- [7] a) Y. Yu, Y. Li, X. Wang, H. Nian, L. Wang, J. Li, Y. Zhao, X. Yang, S. Liu, L. Cao, *J. Org. Chem.* **2017**, *82*, 5590–5596; b) X. Ni, S. Chen, Y. Yang, Z. Tao, *J. Am. Chem. Soc.* **2016**, *138*, 6177–6183; c) Q. Zhang, D. Li, X. Li, P. B. White, J. Mecnović, X. Ma, H. Ågren, R. J. M. Nolte, H. Tian, *J. Am. Chem. Soc.* **2016**, *138*, 13541–13550; d) B. Hua, L. Shao, G. Yu, F. Huang, *Chem. Commun.* **2016**, *52*, 10016–10019.
- [8] a) H. Cheng, Z. Li, Y. Huang, L. Liu, H. Wu, *ACS Appl. Mater. Interfaces* **2017**, *9*, 11889–11894; b) B. Jiang, D. Guo, Y. Liu, K. Wang, Y. Liu, *ACS Nano* **2014**, *8*, 1609–1618; c) R. T. K. Kwok, C. W. T. Leung, J. W. Y. Lam, B. Tang, *Chem. Soc. Rev.* **2015**, *44*, 4228–4238; d) J. Mei, N. L. C. Leung, R. T. K. Kwok, J. W. Y. Lam, B. Tang, *Chem. Rev.* **2015**, *115*, 11718–11940.
- [9] a) Z. Chen, Y. Liu, W. Wagner, V. Stepanenko, X. Ren, S. Ogi, F. Würthner, *Angew. Chem. Int. Ed.* **2017**, *56*, 5729–5733; *Angew. Chem.* **2017**, *129*, 5823–5827; b) F. Würthner, T. E. Kaiser, C. R. Saha-Möller, *Angew. Chem. Int. Ed.* **2011**, *50*, 3376–3410; *Angew. Chem.* **2011**, *123*, 3436–3473; c) A. Rödl, B. Ritschel, C. Mück-Lichtenfeld, V. Stepanenko, G. Fernández, *Chem. Eur. J.* **2016**, *22*, 15772–15777; d) A. Liess, A. Lv, A. Arjona-Esteban, D. Bialas, A. Krause, V. Stepanenko, M. Stolte, F. Würthner, *Nano Lett.* **2017**, *17*, 1719–1726.

- [10] a) J. Lagona, P. Mukhopadhyay, S. Chakrabarti, L. Isaacs, *Angew. Chem. Int. Ed.* **2005**, *44*, 4844–4870; *Angew. Chem.* **2005**, *117*, 4922–4949; b) L. Isaacs, *Acc. Chem. Res.* **2014**, *47*, 2052–2062; c) G. Ghale, W. M. Nau, *Acc. Chem. Res.* **2014**, *47*, 2150–2159; d) W. M. Nau, G. Ghale, A. Hennig, H. Bakirci, D. M. Bailey, *J. Am. Chem. Soc.* **2009**, *131*, 11558–11570; e) S. J. Barrow, S. Kasera, M. J. Rowland, J. Barrio, O. A. Scherman, *Chem. Rev.* **2015**, *115*, 12320–12406.
- [11] a) D. Guo, Y. Liu, *Acc. Chem. Res.* **2014**, *47*, 1925–1934; b) Y. Wang, Y. Zhang, Y. Liu, *J. Am. Chem. Soc.* **2015**, *137*, 4543–4549; c) M. Lee, D. Quang, H. Jung, J. Yoon, C. Lee, J. Kim, *J. Org. Chem.* **2007**, *72*, 4242–4245.
- [12] Z. Zhang, Y. Zhang, Y. Liu, *J. Org. Chem.* **2011**, *76*, 4682–4685.
- [13] a) I. Shulov, R. V. Rodik, Y. Arntz, A. Reisch, V. I. Kalchenko, A. S. Klymchenko, *Angew. Chem. Int. Ed.* **2016**, *55*, 15884–15888; *Angew. Chem.* **2016**, *128*, 16116–16120; b) Y. Wang, Y. Zhang, Y. Wang, Y. Liu, *Chem. Mater.* **2015**, *27*, 2848–2854.
- [14] K. Wang, Y. Chen, Y. Liu, *Chem. Commun.* **2015**, *51*, 1647–1649.

Manuscript received: June 26, 2018

Accepted manuscript online: August 11, 2018

Version of record online: August 23, 2018